18TH WORLD CONFERENCE ON EARTHQUAKE ENGINEERING
WCEE2024
MILAN

MILAN, ITALY
30TH JUNE - 5TH JULY 2024

www.wcee2024.it

LIDAR-BASED ASSESSMENT OF EARTHQUAKE-INDUCED BUILDING DAMAGE: THE NAPA CASE STUDY

F. Foroughnia[1], V. Macchiarulo[1], L. Berg[2], M. DeJong[2], P. Milillo[3,4], K.W. Hudnut[5], K. Gavin[1], & G. Giardina[1]

[1] Department of Geoscience and Engineering, Delft University of Technology, Delft, The Netherlands

[2] Department of Civil and Environmental Engineering, University of California, Berkeley, Berkeley, United States

[3] Department of Civil and Environmental Engineering, University of Houston, Houston, United States

[4] Microwave and Radar Institute, German Aerospace Center (DLR), Weßling, Germany

[5] Southern California Edison, Rosemead, United States

Abstract: *Earthquakes can result in significant human and economic losses, primarily caused by building collapses over vast areas. It is crucial to identify and assess structural damage on a regional scale to effectively respond to emergencies and manage post-disaster scenarios. Typically, the evaluation of structural damage involves labour-intensive inspections of individual buildings during field reconnaissance missions conducted after earthquakes. These missions can be costly and time-consuming, particularly when large areas require investigation Remote sensing techniques offer a cost-effective alternative to on-site inspections by providing frequent observations over vast regions. However, existing remote sensing techniques have limitations in identifying damage beyond severe or complete building collapses. These techniques typically rely on qualitative observations of building shape and regularity derived from satellite imagery, failing to incorporate structural information about the building response. As a result, quantitative assessment of damage and the detection of moderate levels of damage remain challenging. In this study, we propose a new methodology that uses building displacements as key indicators of the building response to earthquakes, enabling a quantitative assessment of damage. Airborne Light Detection And Ranging (LiDAR) data acquired before and after an earthquake were used to estimate seismic-induced building displacements. Then, the LiDAR-based building displacements were integrated with structural damage indicators to quantify building damage levels. To validate the proposed approach, we applied it to analyse 684 buildings affected by the 2014 South Napa earthquake in California. Results showed that most structures experienced slight to moderate damage, indicating good agreement with in-situ observations. This work highlights the potential of remote sensing LiDAR data in accurately quantifying damage levels and facilitating effective disaster management.*

1. Introduction

Earthquakes are one of the most threatening hazards in the world, causing human and economic losses. The most impactful damage is often due to structural collapses as a result of earthquake-induced ground shaking. This emphasises the need for post-earthquake structural damage assessment to aid the rescue process and the identification of buildings that need to be access-restricted for safety purposes (Macabuag et al., 2022).

Typically, engineers perform time-consuming and expensive building-by-building inspections during post-earthquake field reconnaissance missions (Whitworth et al., 2022), limiting assessments to sparse observations. A more cost-effective and widespread solution is offered by remote sensing techniques, which provide frequent, extensive observations over large regions (Voigt et al., 2007). These techniques primarily rely on post-event data classification and multi-temporal change detection analysis to identify damaged structures. Classification-based methods involve analysing post-earthquake satellite imageries to distinguish between damaged and undamaged buildings (Du et al., 2020, Eslamizade et al., 2021), while change detection methods use satellite data collected before and after the seismic event to identify significant changes in the environment (Karimzadeh et al., 2018). These methods are often combined with a categorisation process to classify the observed changes into distinct damage levels (Giardina et al., 2023).

Although these techniques succeed in distinguishing between collapsed and undamaged buildings, they fail to quantify the intermediate damage levels, especially in case of slight to moderate damage. A more effective approach involves measuring building displacements, which are directly linked to building deformations and can provide insights into failure mechanisms. Differential LiDAR-based approaches can be used to measure building displacements. Among these approaches, Iterative Closest Point (ICP) can align two 3D point clouds acquired at different times by minimising the distance between the clouds (Besl and McKay, 1992, Chen and Medioni, 1992). The ICP method can be used to estimate building displacements by aligning two sets of building point clouds acquired before and after an earthquake.

In this study, we developed a new methodology to quantitatively assess earthquake-induced structural damage by using building displacements derived from LiDAR remote sensing data in integration with structural analysis. LiDAR datasets acquired before and after the 2014 South Napa earthquake were used to test the proposed assessment method, and results were compared with field surveys (Hudnut et al., 2014, Cal OES, 2014).

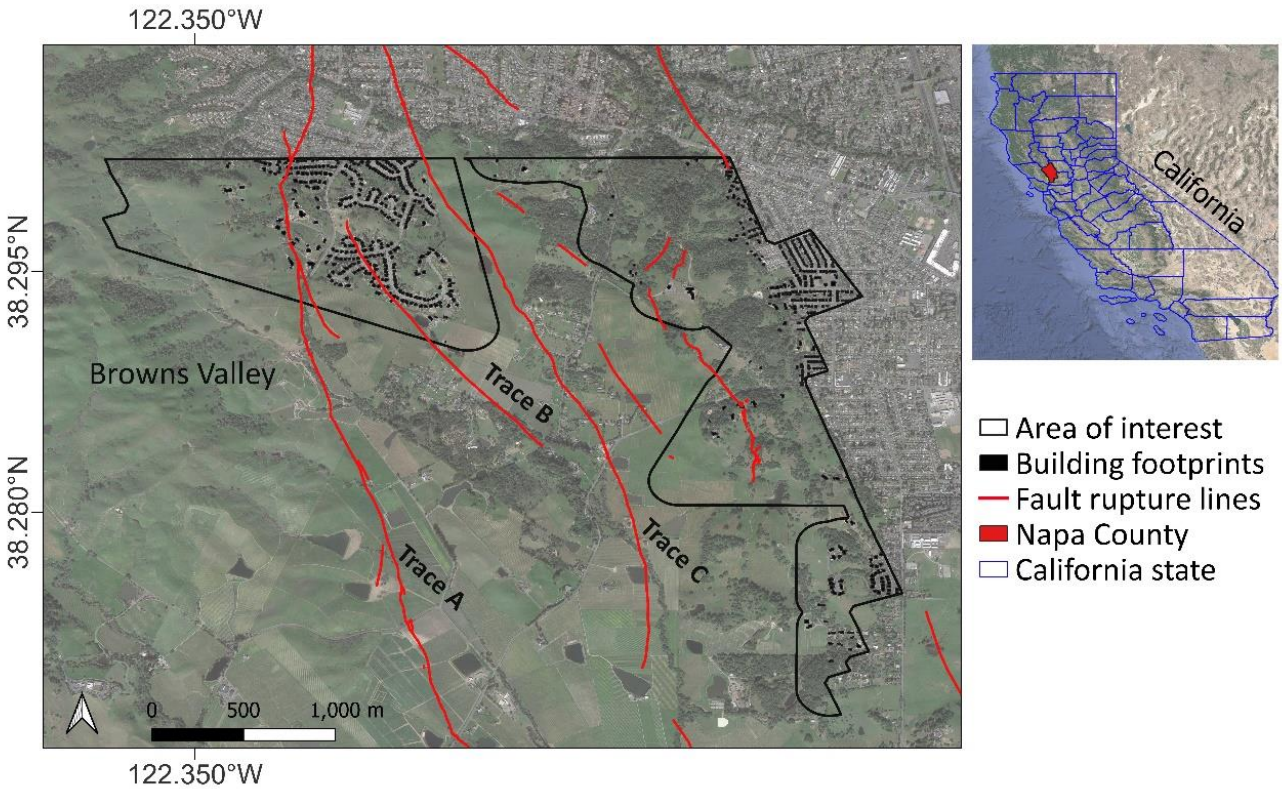

Figure 1. Case study area, showing the regions covered by pre- and post-event LiDAR data. Red lines indicate fault ruptures (Ponti et al., 2019). The black polygons refer to building footprints, obtained from OpenStreetMap (OSM) (OpenStreetMap, 2020) and the Napa municipality (County of Napa, 2021).

2. Case study and datasets

On August 24, 2014, a magnitude Mw 6.0 earthquake occurred north of San Francisco, causing significant damage in the area, including the city of Napa. The epicentre was located at the southern end of Napa Valley at a depth of 10km, roughly 8km southwest of Napa, California. The earthquake caused fractures along several strands of the West Napa fault zone, spanning from nearly 12 to 15km from the town of Cuttings Wharf in the south to outside the northern boundary of Alston Park in the city of Napa (Figure 1).Co-seismic slip ranged from 1.5 to 46 cm along the earthquake rupture (Brocher et al., 2015). After slip varied up and down the fault, ranging from 10−20 mm per day in some locations to just over 40 mm in Browns Valley after 60 days (Hudnut et al., 2014).

A pre-earthquake LiDAR dataset was collected over Napa County on June 7th, 2014, using a Leica ALS60 with a nominal point density of 8 pts/m2. Following the earthquake rupture in August, a post-earthquake dataset was acquired by an Optech Orion M300 scanner with a point density of ~ 11.4 pts/m2 (Lyda et al., 2016). The study presented in this paper focuses on the overlapping area covered by both surveys, equal to approximately 4.7 km^2.

We used field measurements of lateral ground offsets collected by the U.S. Geological Survey (USGS) team to validate the bare-ground displacements derived by LiDAR data. Structural damage estimated from the Lidar displacements was compared with on-site building damage assessment conducted by the California Governor's Office of Emergency Services (Cal OES) (Cal OES, 2014). Cal OES tagged buildings with yellow to indicate usage restrictions and red to signify they were unsafe for occupancy.

3. Methodology

The proposed method integrates building displacements obtained from LiDAR data with structural analysis to estimate drift measurements, serving as an indicator of damage. Figure 2 shows a schematic summary of the method.

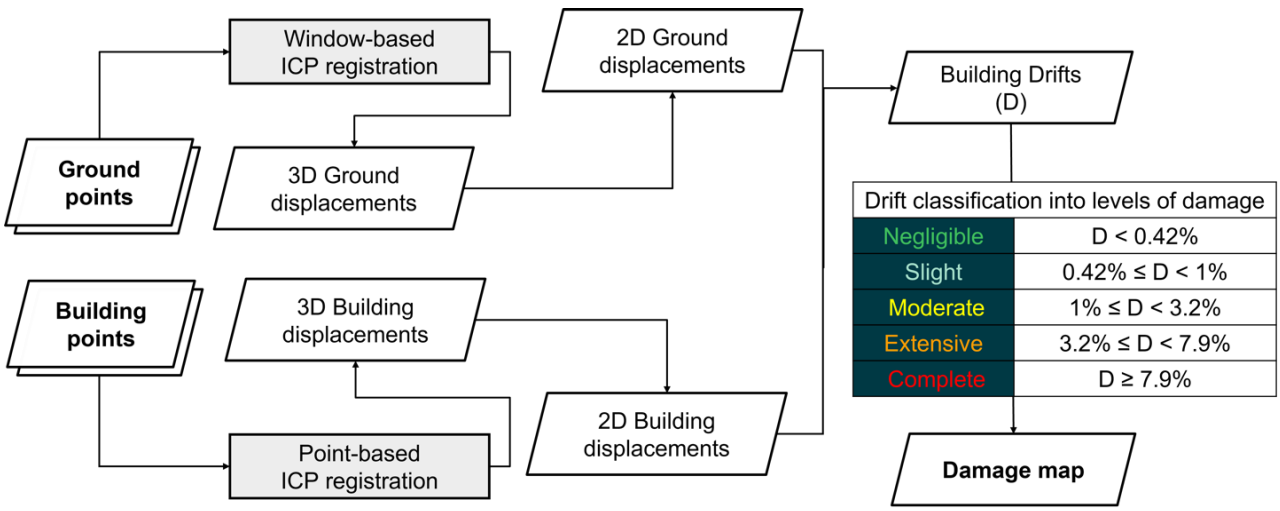

Figure 2. Flowchart of the proposed method.

LiDAR is an active remote sensing technology, using the near-infrared range of the electromagnetic spectrum to acquire data of the Earth's surface. LiDAR sensors emit a laser pulse toward the ground surface and record the time it takes for the pulse to return to the sensor. This process yields distance measurements, allowing for the precise calculation of 3D coordinates for Earth features represented in point cloud forms. In addition to the scanner, a LiDAR system includes positioning and navigation devices, such as the Global Positioning System (GPS) and Inertial Measurement Unit (IMU), to determine the absolute position and rotation of the sensor (NOAA, 2012).

Airborne LiDAR point clouds can be processed through the ICP technique to retrieve seismic deformations (Nissen et al., 2012, Scott et al., 2018, Lyda et al., 2016, Zhang, 2016). The main idea behind using ICP registration for seismic displacement analysis is that the vectors aligning pre- and post-earthquake clouds represent ground surface movements.

The method designates one of the clouds as a fixed reference and iteratively aligns the other cloud to the reference cloud through a repetitive alignment procedure. First, for every point in the second cloud, a corresponding point is identified in the reference cloud based on the nearest Euclidean distance. Second, a rigid body transformation, comprising a translation vector and a rotation matrix, is applied to the second cloud. This transformation aims to minimise the Mean Square Error (MSE) between all corresponding pairs. As the correspondences between points progressively improve, the second point cloud iteratively moves closer to being aligned with the reference cloud. This process continues until the MSE either stabilizes (no further change) or reaches a predetermined threshold.

In this study, we classified bare ground and building LiDAR points based on their height information. The ICP registration method was then applied to the pre- and post-event bare ground point clouds to obtain the bare ground displacements. We performed a window-based ICP registration (Nissen et al., 2012). As the ground displacements might be spatially different from near-fault areas to more distant locations, we split datasets into windows so that each window is transformed separately. We used window size of 100m and step size of 25m (Zhang, 2016) to register the bare ground point clouds. To exclude misclassification points and outliers, we added a rejection step based on the distance and normal vector compatibility criteria to exclude invalid correspondences from the ICP processing chain.

The point observations of each building roof from before and after the earthquake were also aligned to estimate the total building displacements. We extracted points within a buffer around each building to estimate an average bare ground displacement value. We then subtracted the amount of averaged bare ground displacements from the total building displacement vectors, to estimate the building residual displacements. In the next step, the maximum value of the residual displacement of each structure was divided by the building height to obtain drift ratios, D (Pitilakis et al., 2014). The damage level was then categorised as negligible for D < 0.42%, slight for 0.42% ≤ D < 1%, moderate for 1% ≤ D < 3.2%, extensive for 3.2% ≤ D < 7.9%, and complete for D ≥ 7.9% (FEMA, 2006).

4. Results

Figure 3 illustrates the bare ground displacement maps obtained from the ICP registration method. According to Figure 3 (a-c), some areas exhibit significant displacements, indicated by dark blue or bright yellow colours. These regions correspond to locations where no post-event data is available, causing the method to identify incorrect corresponding point in the reference data cloud. To address this issue, an additional rejection step was added to the ICP chain, excluding corresponding pairs with distance greater than 30 cm and normal angle exceeding the average normal angles within the paired window. Figure 3 (b-d) illustrate the corrected ground displacement maps after applying the rejection step. The Y component shows larger displacements, with positive displacement on the left side and negative displacement on the right side of the fault rupture, respectively. This aligns with the seismic behaviour observed in the area of interest, characterized as right lateral strike-slip. Furthermore, our study aligns with the findings of other studies in the Browns Valley region, such as the research conducted by Lyda et al. (2016). Their work identified similar ground displacement in terms of both direction and magnitude. However, their results indicated certain areas where the ground moved in the same direction on both sides of the main rupture. In contrast, our study delineates a distinct difference in the displacement pattern, accurately indicating the location of the fault rupture.

To calculate the residual movements for each building, it was necessary to remove the ground movement components from the total building displacements. To achieve this, a 4m buffer zone was applied around each building footprint to extract the average ground displacements beneath the corresponding structure. Then, the average ground values were subtracted from the total building displacements to estimate the residual displacements. These residual displacements were then used to obtain the drift ratios and implement the damage classification. The distribution of obtained damage levels is illustrated in Figure 4, which shows that the majority of buildings exhibited moderate levels of damage, with only a few suffering severe damage.

We validated the bare-ground displacements through comparison with the field observations collected by the USGS team (Hudnut et al., 2014). The USGS team measured right-lateral offsets along the fault strands at various locations. Within all the observations along trace A, only one offset observation of 36 cm is included in our study area (Figure 5).

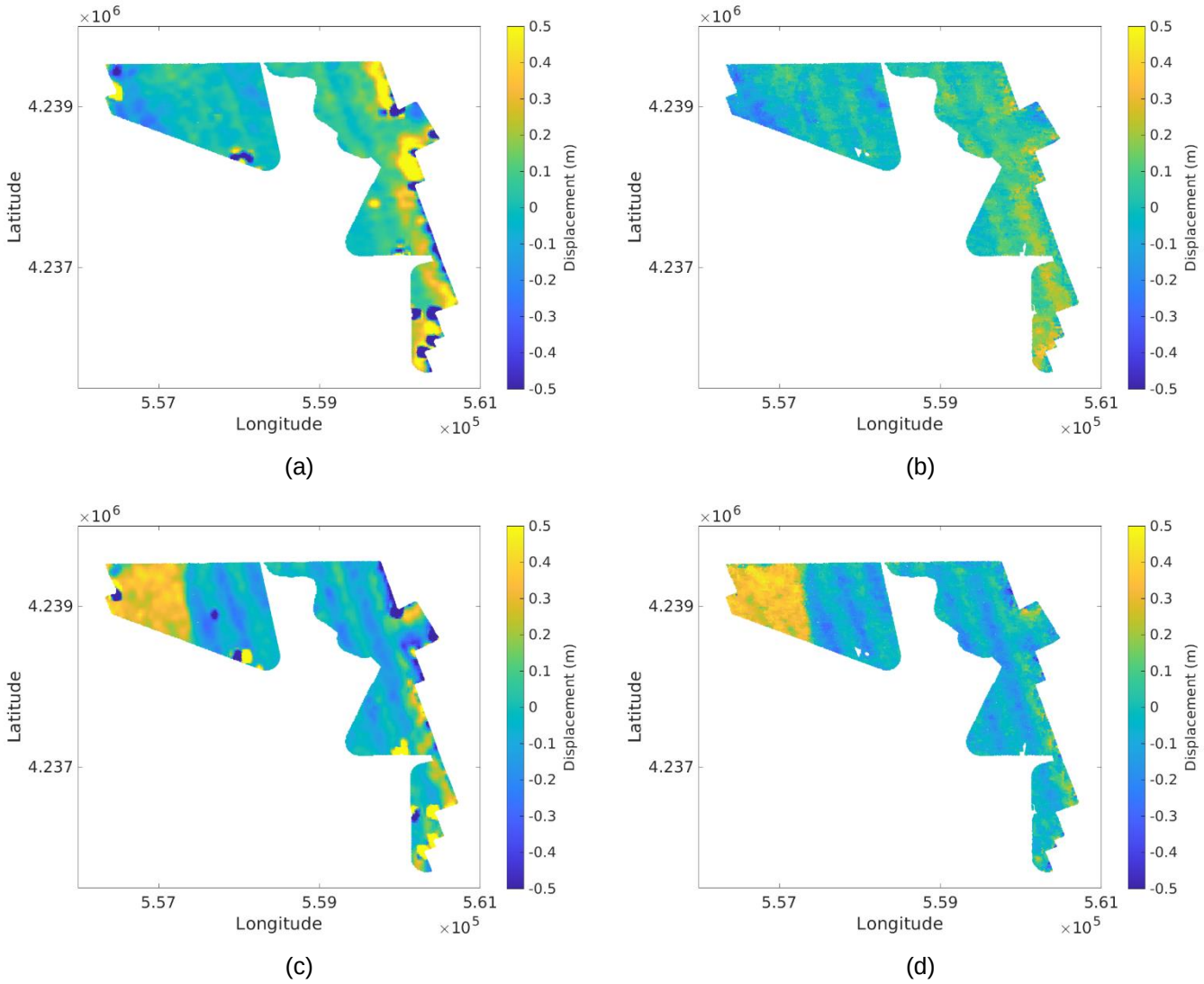

Figure 3. LiDAR-derived bare ground displacement maps in (a) X, and(c) Y directions. Figures (b) and (d) show the corresponding maps where false pairs were removed.

As the precise location of this measurement was unspecified, we analysed a range of displacement values along the fault strand in a nearby area. This led to the creation of three perpendicular cross-sections, each stretching 200 m, placed at 50 m intervals. To estimate the cross-sectional displacement, we defined a 1m-wide buffer zone on either side of each cross-section. Within these buffer zones, we identified displacement points in the Y-direction. We then computed the average Y-direction displacement magnitudes on each side of the cross-section. To determine the Y-direction displacement offset for each cross-section, we calculated the difference between the average magnitude on the right side and the average magnitude on the left side. Since the LiDAR measurements were in geographical coordinates, the LiDAR-derived offsets correspond to displacements along the North-South direction. Thus, to compare these offsets with the field observations, we projected the LiDAR-derived offsets onto the fault direction using the angle between the offset displacement vector and the fault line. The average magnitude of LiDAR-derived offsets projected along the fault rupture was found to be 35.9 cm, showing a good agreement between the LiDAR analysis and the in-situ observation.

To validate the building-level results, we used information from buildings that were tagged by the Cal OES (Cal OES, 2014). 38 yellow-tagged and 1 red-tagged buildings were included in our area of interest. As shown in Table 1, results indicate a strong correspondence between the moderate levels of damage inferred from the LiDAR analysis and the yellow-tagged buildings.

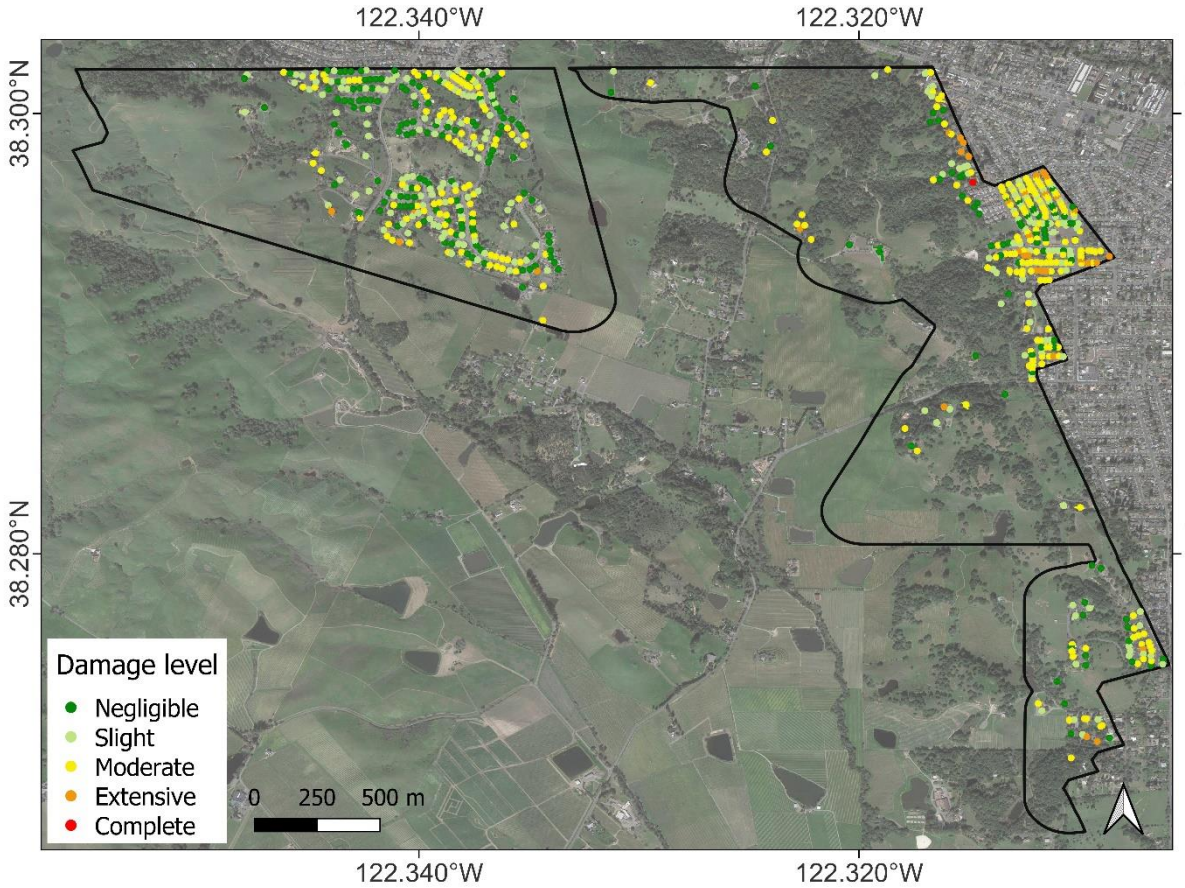

Figure 4. Building damage map. Building damage levels are based on the residual drift ratios derived from LiDAR displacement measurements.

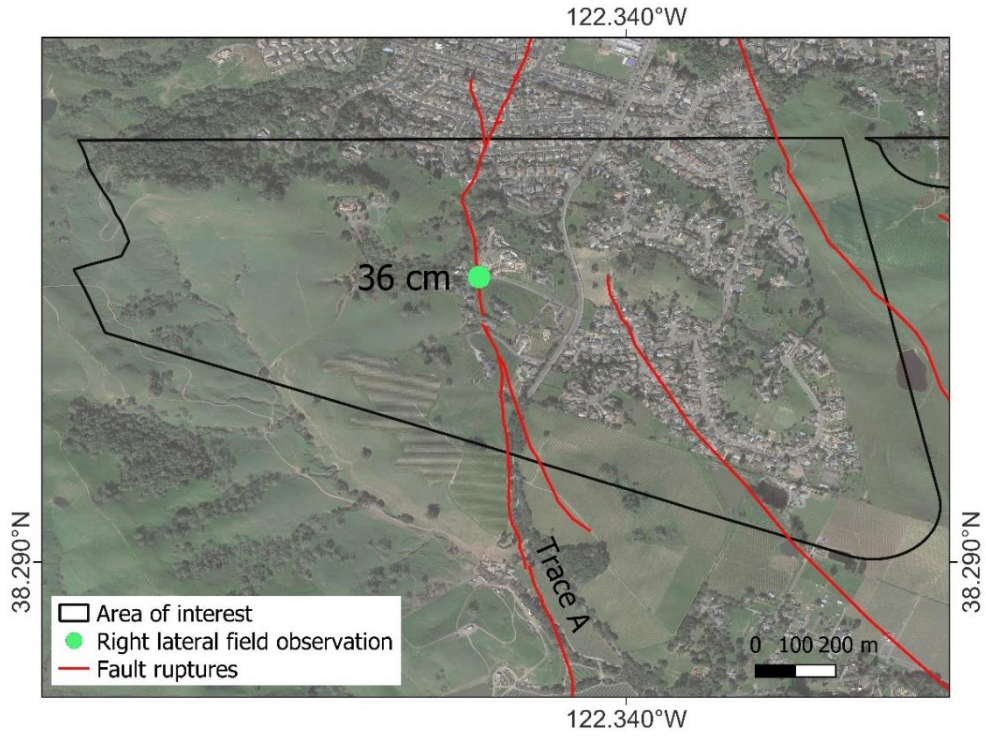

Figure 5. In-situ right-lateral displacements along trace A.

Table 1. Distribution of LiDAR-based damage levels for the 38 yellow-tagged buildings in the area of interest.

Damage level	No. of buildings
Negligible	12
Slight	6
Moderate	19
Extensive	1
Complete	0

5. Conclusion

This study introduces a new method for assessing earthquake-induced building damage on a regional scale, using remote sensing LiDAR point cloud data in combination with structural engineering parameters. By using the ICP registration technique, we estimated the displacements of buildings and the ground, to obtain building drifts and categorise damage levels. The method was applied to assess the buildings affected by the 2014 South Napa earthquake in California, confirming its capability to detect slight to moderate damage levels, which are often challenging to identify. This study highlights the potential of the integration of LiDAR-based displacement measurements with structural analysis methods, offering a more accurate approach to post-earthquake damage assessment over vast regions.

6. References

BESL, P. J. & MCKAY, N. D. (Year) Published. Method for registration of 3-D shapes. Sensor fusion IV: control paradigms and data structures, 1992. Spie, 586-606.

BROCHER, T. M., BALTAY, A. S., HARDEBECK, J. L., POLLITZ, F. F., MURRAY, J. R., LLENOS, A. L., SCHWARTZ, D. P., BLAIR, J. L., PONTI, D. J. & LIENKAEMPER, J. J. (2015). The M w 6.0 24 August 2014 South Napa earthquake. *Seismological Research Letters,* 86**,** 309-326.

CAL OES. (2014). *August 24, 2014 south napa earthquake* [Online]. Available: https://www.caloes.ca.gov/ [Accessed].

CHEN, Y. & MEDIONI, G. (1992). Object modelling by registration of multiple range images. *Image and vision computing,* 10**,** 145-155.

COUNTY OF NAPA. (2021). *Gis data catalog* [Online]. Available: http://gis.napa.ca.gov/giscatalog/ [Accessed].

DU, Y., GONG, L., LI, Q. & WU, F. (Year) Published. Earthquake-induced building damage assessment on SAR multi-texture feature fusion. IGARSS 2020-2020 IEEE International Geoscience and Remote Sensing Symposium, 2020. IEEE, 6608-6610.

ESLAMIZADE, F., RASTIVEIS, H., ZAHRAEE, N. K., JOUYBARI, A. & SHAMS, A. (2021). Decision-level fusion of satellite imagery and LiDAR data for post-earthquake damage map generation in Haiti. *Arabian Journal of Geosciences,* 14**,** 1-16.

FEMA (2006). Multi-hazard loss estimation methodology, earthquake model. Federal Emergency Management Agency, Washington, D.C.

GIARDINA, G., MACCHIARULO, V., FOROUGHNIA, F., JONES, J. N., WHITWORTH, M. R., VOELKER, B., MILILLO, P., PENNEY, C., ADAMS, K. & KIJEWSKI-CORREA, T. (2023). Combining remote sensing techniques and field surveys for post-earthquake reconnaissance missions. *Bulletin of Earthquake Engineering***,** 1-25.

HUDNUT, K. W., BROCHER, T. M., PRENTICE, C. S., BOATWRIGHT, J., BROOKS, B. A., AAGAARD, B. T., BLAIR, J. L., FLETCHER, J. P. B., ERDEM, J. & WICKS JR, C. W. (2014). Key recovery factors for the August 24, 2014, South Napa earthquake. US Geological Survey.

KARIMZADEH, S., MATSUOKA, M., MIYAJIMA, M., ADRIANO, B., FALLAHI, A. & KARASHI, J. (2018). Sequential SAR coherence method for the monitoring of buildings in Sarpole-Zahab, Iran. *Remote Sensing,* 10**,** 1255.

LYDA, A., ZHANG, X., GLENNIE, C., HUDNUT, K. & BROOKS, B. (2016). Airborne light detection and ranging (lidar) derived deformation from the MW 6.0 24 August, 2014 South Napa earthquake estimated by two and three dimensional point cloud change detection techniques. *The International Archives of the Photogrammetry, Remote Sensing and Spatial Information Sciences,* 41**,** 35-42.

MACABUAG, J., ALTHEIM, C., THORVALDSDOTTIR, S. & PERKS, D. (2022). Damage assessments by International Engineers following the Albania earthquake of November 2019. *International Journal of Disaster Risk Reduction,* 72**,** 102822.

NISSEN, E., KRISHNAN, A. K., ARROWSMITH, J. R. & SARIPALLI, S. (2012). Three‐dimensional surface displacements and rotations from differencing pre‐and post‐earthquake LiDAR point clouds. *Geophysical Research Letters,* 39.

NOAA, N. O. A. A. A. N. C. S. C. (2012). Lidar 101: An Introduction to Lidar Technology, Data, and Applications. *In:* REVISED. (ed.). Charleston, SC: NOAA Coastal Services Center.

OPENSTREETMAP. (2020). Available: https://www.openstreetmap.org/#map=14/33.7216/-117.7676 [Accessed].

PITILAKIS, K., CROWLEY, H. & KAYNIA, A. M. (2014). SYNER-G: typology definition and fragility functions for physical elements at seismic risk. *Geotechnical, Geological and Earthquake Engineering,* 27**,** 1-28.

SCOTT, C. P., ARROWSMITH, J. R., NISSEN, E., LAJOIE, L., MARUYAMA, T. & CHIBA, T. (2018). The M7 2016 Kumamoto, Japan, earthquake: 3‐D deformation along the fault and within the damage zone constrained from differential lidar topography. *Journal of Geophysical Research: Solid Earth,* 123**,** 6138-6155.

VOIGT, S., KEMPER, T., RIEDLINGER, T., KIEFL, R., SCHOLTE, K. & MEHL, H. (2007). Satellite image analysis for disaster and crisis-management support. *IEEE transactions on geoscience and remote sensing,* 45**,** 1520-1528.

WHITWORTH, M. R., GIARDINA, G., PENNEY, C., DI SARNO, L., ADAMS, K., KIJEWSKI-CORREA, T., BLACK, J., FOROUGHNIA, F., MACCHIARULO, V. & MILILLO, P. (2022). Lessons for remote post-earthquake reconnaissance from the 14 August 2021 Haiti earthquake. *Frontiers in Built Environment,* 8.

ZHANG, X. (2016). *LiDAR-Based Change Detection for Earthquake Surface Ruptures.*